ELSEVIER

Polymer 43 (2002) 4733–4743

polymer

www.elsevier.com/locate/polymer

Oxygen solubility and specific volume of rigid amorphous fraction in semicrystalline poly(ethylene terephthalate)

J. Lin, S. Shenogin, S. Nazarenko*

Department of Macromolecular Science, Center for Applied Polymer Research, Case Western Reserve University, Cleveland, OH 44106-7202, USA

Received 23 January 2002; received in revised form 6 April 2002; accepted 12 April 2002

Abstract

The existence of rigid amorphous fraction (RAF) in semicrystalline poly(ethylene terephthalate) (PET) is associated with the lamellar stack crystalline morphology of this polymer, the regions where several crystalline lamellas are separated by very thin (20–40 Å) amorphous layers. In contrast, regular or mobile amorphous fraction is associated with much thicker interstack regions. The oxygen transport properties of PET isothermally crystallized from the melt (melt-crystallization) or quenched to the glassy state and then isothermally crystallized by heating above T_g (cold-crystallization) were examined at 25 °C. Explanation of unexpectedly high solubility of crystalline PET was attributed to the formation of RAF, which in comparison with mobile amorphous phase is constrained and vitrifies at much higher than T_g temperature thus developing an additional excess-hole free volume upon cooling. Measurements of crystallinity and jump in the heat capacity at T_g were used to determine the amount of mobile and rigid amorphous fractions. Overall oxygen solubility was associated with the solubility of mobile and rigid amorphous fractions. The oxygen solubility of the RAF was determined and related to the specific volume of this fraction. The specific volume of the RAF showed a direct correlation with the crystallization temperature. It was shown that upon crystallization from either melt or glassy state, the constrained between crystalline lamellas PET chains consisting of the RAF, vitrify at the crystallization temperature and resemble the glassy behavior despite high temperature. When cooled to room temperature, the RAF preserves a memory about the melt state of polymer, which is uniquely defined by the crystallization temperature.

Keywords: Semicrystalline poly(ethylene terephthalate); Rigid amorphous fraction; Oxygen solubility and specific volume

1. Introduction

Poly(ethylene terephthalate) (PET) demonstrates an excellent combination of important for packaging applications properties such as easy processing, good mechanical properties, transparency, and reasonably high resistance to oxygen and carbon dioxide. However, there is a continuous practical need to improve PET gas barrier properties. Crystallization, in particular cold-crystallization from the glassy state, is traditionally considered as one of the most practical and simple approaches to improve gas barrier. Therefore, understanding of gas transport behavior of crystalline PET is important. Gas transport behavior of semicrystalline PET has been studied in the past [1–3].

As in the case of most of the semicrystalline polymers, PET exhibits a decrease of gas permeability with crystallinity. This effect is explained in terms of two factors [1,4]. First, inclusion of impermeable crystallites decreases the amount of amorphous material through which gas molecules can permeate. Second, impermeable crystallites increase the tortuosity of the transport path (geometric impedance). The former affects total solubility of the permeant in the material, the later affects the diffusion coefficient. About 30 years ago, Michaels et al. [2] first pointed out that gas solubility in cold-crystallized semicrystalline PET is reduced, but not in direct proportion with the decrease in amorphous volume as expected. The decrease of solubility with crystallinity was essentially smaller than expected from the increase of crystallinity. They proposed that crystallization tended to occur in the denser regions of the amorphous matrix, thereby effectively concentrating the microvoids in the remaining amorphous regions. Oxygen transport in cold-crystallized PET was recently reexamined by Sekelik et al. [3]. They also observed the effect previously reported by Michaels et al. Larger than expected oxygen solubility in semicrystalline PET was related in this work with the decrease of the

* Corresponding author.
E-mail address: sin@po.cwru.edu (S. Nazarenko).

0032-3861/01/$ - see front matter
PII: S0032-3861(02)00278-1

average amorphous density with crystallinity (dedensification) resulted from the conformational restrictions imposed by crystallinity on polymer chains in the amorphous phase. Sekelik et al. employed the modified two-phase model, first proposed for semicrystalline PET by Bornschlegl and Bonart [5] in order to interpret the solubility data. This phenomenological model traditionally considered only two phases in semicrystalline PET amorphous and crystalline. However, it was assumed that the density of the amorphous phase changes with crystallinity thus to be a function of overall density. Bornschlegl and Bonart experimentally measured the dependence of amorphous density in semicrystalline PET versus overall density and confirmed that the amorphous density decreased with the increase of overall density upon crystallization. This result, however, failed to explain whether the amorphous density in semicrystalline PET changes with crystallinity homogeneously, or it changes heterogeneously being a direct consequence of the heterogeneous nature of the crystalline morphology in general. It seems reasonable to anticipate that the amorphous regions, which are located either in the close proximity to the crystalline boundaries or constrained between the neighboring crystalline lamellas, should be affected stronger by crystallinity than those located far away from crystals.

About 15 years ago, the concept of third phase or fraction, rigid amorphous fraction (RAF), in addition to crystalline phase and mobile amorphous fraction (MAF), was first introduced to explain the vivid deviation from one-to-one correspondence between crystallinity and jump in heat capacity in the glass transition interval for several semi-flexible polymers containing phenylene groups such as PET [6–12]. RAF represents the fraction of amorphous phase that does not contribute to jump in heat capacity. It was suggested that RAF might contain molecules, whose mobility is hindered in the presence of crystallinity. The existence of RAF was often associated with the existence in the crystalline structure of the lamella stacks, the regions where the crystalline lamellas are separated by very thin (20–40 Å) amorphous layers. Much thicker (100–2000 Å) amorphous layers separate the lamella stacks [13,14]. It was suggested that RAF morphologically is associated with the interlamellar regions, while MAF, which behaves normally and contributes to the glass transition, is associated with the interstack amorphous regions [15].

Though the existence of RAF seems to be experimentally well demonstrated [6–12,16], probing of the properties of this phase is under current scrutiny. One of the most important questions is what is the chain packing in the RAF and how it is different from that in the regular or MAF. It is also interesting whether the chain packing in RAF is defined by crystallization conditions (crystallization temperature, pressure), or it is also defined by crystalline morphology. Schick et al. [17] demonstrated that RAF in semicrystalline PET does not exhibit a separate T_g in the entire temperature range up to the melting transition, while the parameters of sub-T_g relaxation for RAF and MAF are essentially the same. Recently, using temperature-modulated DSC, Schick et al. [18] also showed that similar phenomenon takes place for several other slowly crystallizing polymers such as bisphenol-A polycarbonate and poly(3-hydroxybutyrate). No changes in the amount of RAF occurred in the temperature range between crystallization and the glass transition. Therefore, Schick et al. suggested that the amorphous chains constrained between the crystalline lamellas in PET become effectively vitrified upon crystallization despite a high temperature, while the rest of the amorphous chains located between the lamella stacks continue to be in the melt state. Therefore, the crystallization temperature, T_c, has to be considered as an effective vitrification temperature for RAF. Devitrification of RAF then should occur upon melting of the crystalline lamellas consisting of the lamella stacks.

If this hypothesis is right, the specific volume, $v = 1/\rho$ (ρ is the density), characterizing RAF and MAF have to be essentially different below the crystallization temperature. Fig. 1 exhibits a sketch to illustrate this point. This sketch basically shows a hypothetical thermal expansion behavior associated with RAF and MAF for PET crystallized at some arbitrary crystallization temperature, T_c. Above T_c, in the state of equilibrium melt, the specific volumes for RAF and MAF are apparently the same. If vitrification of RAF occurs at T_c, the slope of specific volume versus temperature for this phase should change at T_c, and become the one, which is a characteristic of the glassy state in the temperature interval below T_c. In turn for MAF, the slope of specific volume versus temperature, below T_c, should continue to be the same as for equilibrium melt and change only at real T_g. Therefore, if the room temperature (RT) is considered as the reference, the specific volume (density) for RAF at RT must be larger (smaller) than that for MAF. Moreover, it is also clear from this scheme that the specific volume of RAF measured at RT should then be a direct function of crystallization temperature.

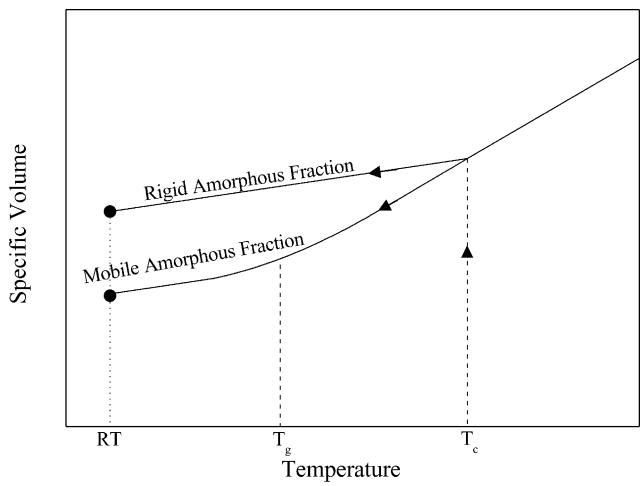

Fig. 1. Schematic plot of specific volume as a function of temperature for rigid and MAFs.

It is widely accepted that vitrification of amorphous polymer is associated with the formation of excess-hole free volume, packing defects effectively frozen in the structure of polymer due to drastic restriction of the macromolecular segmental mobility. These defects (molecular size holes) act as the adsorption sites where gas sorption is considerably stronger than in the dense polymer matrix [19]. Therefore, larger gas solubility was expected for RAF than for MAF according to the Schick's hypothesis as a result of larger specific volume at RT. This behavior could explain why gas solubility in semicrystalline PET did not decrease in the direct proportion with crystallinity.

The main goal of this work was to employ oxygen gas solubility in order to explore the packing of polymer chains in RAF and compare it with that in MAF.

2. Experimental

PET with 2.6 mol% of isophthalic acid (PET-I/2.6), typical commercial PET bottle grade (PET-80), was supplied as pellets by KoSa Corporation, Spartanburg, SC. After being dried in vacuo at 120 °C for 24 h, the pellets were placed in the 6 × 6 in. cavity of a 200 μm-thick spacer and sandwiched between two 8 × 8 in. polished steel platens covered with Teflon-coated aluminum foil. To prepare amorphous PET plaques, the platens were placed in the preheated at 270 °C press and held for 5 min without pressure, then the pressure was increased to 20,000 psi and then, subsequently, released. This cycle was repeated three times to remove the air bubbles from the compression-molded plaques. Finally, the platens were held at 20,000 psi for 5 min and quenched into the ice–water mixture.

For cold-crystallization, the amorphous plaques were first sealed into aluminum foil and annealed in the oil bath for various times, at 110, 140 and 160 °C, and finally quenched into the ice–water mixture. For isothermal melt-crystallization, plaques were first compression molded at 270 °C, as described previously, then the platens with a sample between were rapidly transferred to the convection oven which was preset at crystallization temperature $T_c = 210$ °C. In the oven, the samples were crystallized for various times. After crystallization was completed, the samples were quenched into the ice–water mixture.

Glass transition, melting and crystallization behavior of PET were measured using Perkin–Elmer DSC-7 and Rheometric Scientific SP DSC. The calibration was carried out using indium, tin and sapphire standards. Heating rate 10 °C/min was used over the whole studied temperature range.

Density was measured using gradient column constructed from a solution of calcium nitrate/water in accordance with ASTM-D 1505 Method B. The column was calibrated with glass floats of known density. Small pieces from each plaque (~25 mm^2) were placed in the column and allowed to equilibrate for 15 min before a measurement was taken.

Oxygen flux $J(t)$ at 0% relative humidity was measured using OXTRAN® 2/20 (MOCON) unit, which employs the continuous-flow cell method approved by ASTM (Designation: D 3985-81). This method is generally adopted for measurements of oxygen permeation through polymers. Nitrogen was used as the carrier gas and pure oxygen was used as the test gas. Prior to the test, the film specimen was conditioned in pure nitrogen inside the unit to remove traces of atmospheric oxygen. Conditioning was especially important to measure the non-steady-state oxygen flux from which the diffusion coefficient D was determined. The conditioning was continued until a steady baseline was obtained where the oxygen flux changed by less than 1% during a 20-min test cycle. Then oxygen was introduced to the test cell. The test ended when the flux reached a steady state where the oxygen flux changed by less than 1% during a 20-min test cycle. The bulk thickness l for each specimen was determined after the barrier measurement was completed. A 3 × 3 in. square section was cut from the tested area. The weight W and area A of the cut sample were accurately measured. The bulk thickness was calculated as $l = W/A\rho$, where ρ is measured density. The details of the gas transport measurements adopted in our lab are described elsewhere [3].

3. Results and discussions

3.1. Amorphous phase in semicrystalline PET

Fig. 2 shows typical DSC traces for amorphous,

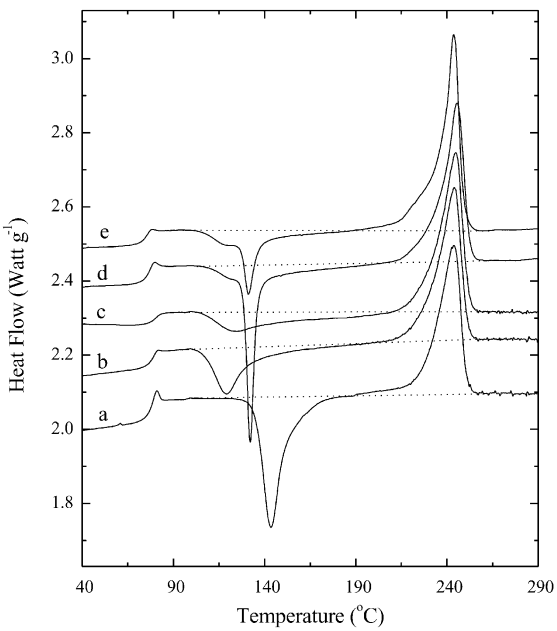

Fig. 2. DSC thermograms of amorphous and semicrystalline PET. (a) amorphous, (b) cold-crystallized at 110 °C (w_c = 13%), (c) cold-crystallized at 110 °C (w_c = 21%), (d) melt-crystallized at 210 °C (w_c = 12%), (e) melt-crystallized at 210 °C (w_c = 21%); (note: the heat capacity scale for the curve (d) is the correct one, all other curves are shifted vertically).

cold-crystallized at 110 °C, and melt-crystallized at 210 °C PET. Amorphous PET showed a glass transition at about 77 °C followed by the cold-crystallization and melting peaks. The glass transition exhibited a characteristic endothermic hysteresis typically observed in the case when cooling to the glassy state and heating rates are not the same [20,21]. Cold-crystallized at 110 °C and melt-crystallized at 210 °C PET exhibited similar, as in the case of amorphous PET, glass transition temperature, however, with less pronounced hysteresis peak. Smaller endothermic hysteresis in the case of semicrystalline polymers is typically reported [7]. Cold-crystallized PET showed a single crystallization peak, which broadened at higher crystallinities. Melt-crystallized PET showed more complex crystallization behavior with a characteristic narrow peak at higher temperatures and a shallow shoulder at lower temperatures. The onset of crystallization in the case of both cold- and melt-crystallized PET was observed at about 100 °C, which was by 20 °C lower than the onset of crystallization peak in the case of amorphous PET. Both cold- and melt-crystallized PET showed the melting peak at about 245 °C.

The heat capacity jump, ΔC_p, at T_g was determined according to the methodology proposed elsewhere [7,21]. The procedure is illustrated in Fig. 3 for glass transition with and without hysteresis. The glass transition point is defined as an intersection of the DSC curve with a median to the two heat capacity lines representing the glass and liquid behavior. At this point apparently a half of the specific heat increment has occurred. The melting (ΔH_m) and cold-crystallization peak (ΔH_{cc}) areas, below and above the dashed baseline (Fig. 2), were measured to calculate the overall heat of fusion, $\Delta H_f = \Delta H_m - \Delta H_{cc}$, which then was used to determine the weight crystalline fraction, $w_c = \Delta H_f / \Delta H_f^0$, where $\Delta H_f^0 = 125$ J g^{-1} is the heat of fusion for 100% crystalline PET [22].

Fig. 4 shows heat capacity jump, ΔC_p, at T_g for cold- and melt-crystallized PET as a function of weight crystalline fraction. The heat capacity jump, ΔC_p, at T_g, is an attribute of the amorphous phase only and must decrease in the direct

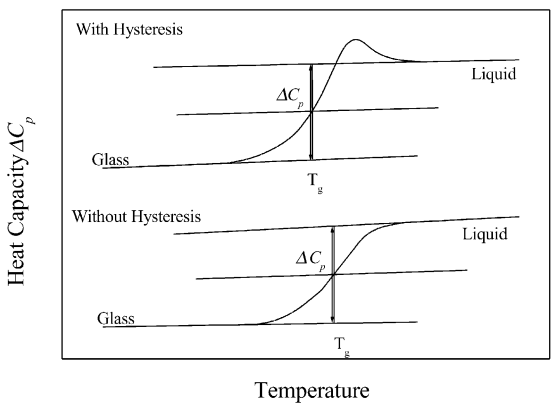

Fig. 3. Procedure of determining the heat capacity jump, ΔC_p, at T_g for glass transition with and without hysteresis.

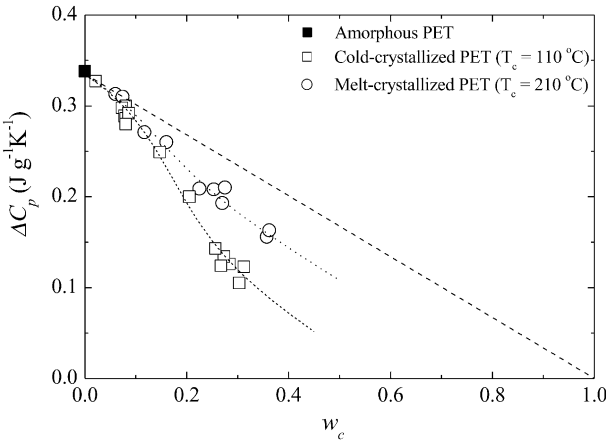

Fig. 4. Heat capacity jump, ΔC_p, at T_g for cold-crystallized at 110 °C and melt-crystallized at 210 °C PET as a function of weight crystalline fraction.

proportion with crystallinity if only two phases, with constant properties, amorphous and crystalline are present (dashed linear trend). However, starting at about 0.1 of the weight crystalline fraction the heat capacity jump for both cold- and melt-crystallized PET showed a strong deviation from that linear trend. The decrease in the heat capacity jump was larger than that predicted by the two-phase model. The heat capacity jump deviation reached its maximum at about 0.25 weight crystalline fraction and then remained the same despite further increase in crystallinity. Cold-crystallized PET showed a stronger deviation from the two-phase linear trend than melt-crystallized PET.

Following the original work of Wunderlich et al. [23,24], the deviation of the heat capacity jump can be used to calculate the weight portion of the rigid amorphous fraction.

$$w_{RAF} = \left[\Delta C_p^a(1 - w_c) - \Delta C_p\right]/\Delta C_p^a = 1 - \Delta C_p/\Delta C_p^a - w_c \quad (1)$$

where ΔC_p^a is the heat capacity jump for the amorphous PET, and $\Delta C_p/\Delta C_p^a$ represents the weight portion of the mobile amorphous fraction, w_{MAF}, which contributes to the jump of heat capacity ΔC_p at T_g. The volume portion of MAF, ϕ_{MAF} can be calculated from the corresponding weight portion, and the densities for an amorphous PET, ρ_a, and semicrystalline PET, ρ, $\phi_{MAF} = w_{MAF}\rho/\rho_a$. The density for amorphous PET is well known $\rho_a = 1.335$ g cm^{-3} [3,25]. Similarly, the volume fraction of crystallinity, ϕ_c, can be calculated from the corresponding weight fraction, and the densities of 100% crystalline PET, ρ_c, and semicrystalline PET, ρ, $\phi_c = w_c\rho/\rho_c$. However, the question what density has to be used for 100% crystalline PET here is less straightforward than in the case of density value for pure amorphous phase. A broad range of densities for 100% crystalline PET (1.455–1.515 g cm^{-3}) has been previously reported [22,26–28].

Fakirov et al. [28] reported probably today the most accurate data regarding the density of crystalline PET. Using WAXS they found the following unit cell dimensions

for the crystalline PET, $a = 4.48$ Å, $b = 5.85$ Å, $c = 10.75$ Å, ($\alpha = 99.5°$, $\beta = 118.4°$, $\gamma = 111.2°$. Negligible differences of the unit cell parameters have been found despite cold crystallizing PET in the broad range of temperatures (120–260 °C). The unit cell parameters were used to calculate the density of crystalline PET, which was found to be 1.515 g cm^{-3}. Therefore, in this work, we used 1.515 g cm^{-3} for the density of 100% crystalline PET. In fact, calculation of the volume fraction of crystalline phase seems to be fairly insensitive to the crystalline density, and basically any value within a broad range of the reported densities could be used. The values of volume fraction of crystalline phase calculated using either of the reported crystalline densities differ by no more than 0.01. This difference is apparently smaller than experimental accuracy in determining the weight fraction of crystallinity from DSC data.

The volume content of RAF can be subsequently calculated from the volume portion of crystallinity and volume portion of MAF, $\phi_{RAF} = 1 - \phi_c - \phi_{MAF}$. Fig. 5(a) and (b) shows the volume fractions of MAF, ϕ_{MAF}, and RAF, ϕ_{RAF}, as a function of volume portion of crystallinity, ϕ_c. As expected, a dependence of ϕ_{MAF} versus ϕ_c (Fig. 5(a)) resembled the same features as a dependence of heat capacity jump versus weight crystalline fraction shown in Fig. 4. The smallest volume portion of MAF for cold-crystallized PET was only 0.38 at 0.25 volume portion of crystallinity. The smallest volume portion of MAF for melt-crystallized PET was 0.5 at 0.35 volume fraction of crystallinity. The amount of MAF for melt-crystallized PET was always larger than for cold-crystallized PET when the samples with the same crystalline fractions were compared. The volume portion of RAF, ϕ_{RAF} (Fig. 5(b)), sharply increased with the volume fraction of crystallinity, ϕ_c, starting at $\phi_c = 0.07$ and then practically leveled off at about $\phi_c = 0.25$ reaching $\phi_{RAF} = 0.37$ for cold-crystallized at 110 °C PET, and $\phi_{RAF} = 0.14$ for melt-crystallized at 210 °C PET.

The larger amount of RAF developed in cold-crystallized PET can be understood assuming that lower crystallization temperatures apparently resulted in the formation of thinner lamellas. So, the number of lamellas in the lamella stacks or, also possibly, the overall number of lamella stacks in cold-crystallized PET was increased compared with those in melt-crystallized PET containing the same crystalline fraction. This presumably could lead to much larger amount of amorphous phase constrained between the crystalline lamellas in the case of cold-crystallized PET.

3.2. Oxygen permeation in semicrystalline PET

Fig. 6 shows typical experimental $J(t)$ curves describing the oxygen flux through the films of amorphous, melt- and cold-crystallized PET measured at RT. Careful conditioning and the appropriate choice of specimen thickness resulted in excellent resolution of the various features of the time dependence. All curves consisted of a non-steady and a steady-state region. The non-steady-state region, associated with the progress of concentration profile across the thickness, is mainly determined by the diffusion coefficient, D. As the permeant concentration in the specimen reached a constant distribution, the flux reached the steady-state value,

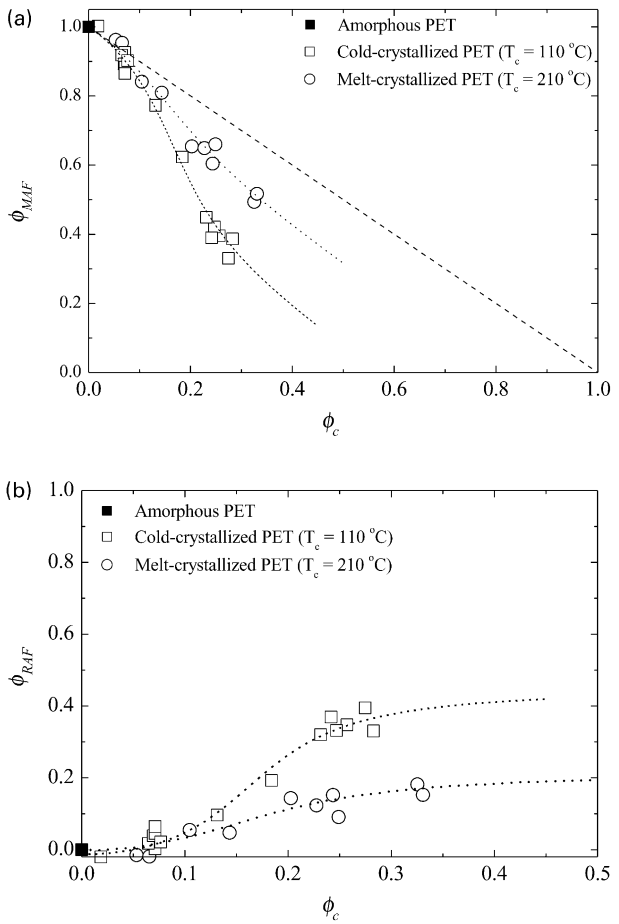

Fig. 5. Volume portions of MAF (a) and RAF (b) versus volume portion of crystallinity for cold-crystallized at 110 °C and melt-crystallized at 210 °C PET.

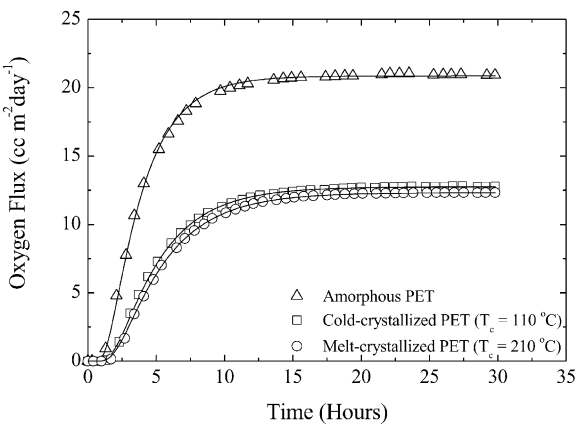

Fig. 6. Experimental oxygen flux versus time data and the fit to Fick's law for amorphous, cold-crystallized at 110 °C ($w_c = 26\%$), and melt-crystallized at 210 °C ($w_c = 23\%$) PET.

J_0. This value normalized by film thickness l and permeant pressure p defined the permeability $P = J_0 l p^{-1}$.

An impermeable phase, such as crystallinity, had a strong effect on both the non-steady-state and steady-state part of the oxygen curve. The non-steady region broadened (slower diffusion), while steady-state permeability decreased with increase in the crystallinity.

In order to obtain the diffusion coefficient and to accurately determine the permeability coefficient, the data were fit to the solution of Fick's second law

$$\frac{\partial c}{\partial t} = D\frac{\partial^2 c}{\partial x^2} \tag{2}$$

with boundary conditions for the permeant concentration $c(x = 0, t) = Sp$; $c(x = l, t) = 0$, where S is the solubility coefficient; p, the gas pressure; l is the sample thickness and initial conditions $c(x, t = 0) = 0$:

$$J(t) = \frac{Pp}{l}\left[1 + 2\sum_{n=1}^{\infty}(-1)^n \exp(-D\pi^2 n^2 t/l^2)\right] \tag{3}$$

Permeability, P, and diffusion coefficient, D, were obtained by performing a two-parametric least square fit of the experimental flux data to Eq. (2). The solubility, S, was obtained from the relationship $P = DS$. The fitting curves are included with the experimental points in Fig. 6. The fits were equally good for all the experiments in this study. From the quality of the fits, it can be concluded that there is no concentration dependence of oxygen at partial gas pressure used in these experiments. As indicated previously, the error in determining the two fitting parameters Pl^{-1} and Dl^{-2}, was estimated not to exceed 2% [3]. Thus the main sources of error in calculating P and D were determined mainly by the accuracy of the bulk average thickness measurements. For this reason, special attention was paid to the bulk average thickness measurement as described in Section 2.

Fig. 7(a)–(c) shows changes in the permeability, diffusion coefficient, and solubility coefficients as a volume fraction of crystallinity. The significant drop in permeability (Fig. 7(a)) with increased crystallinity is usually explained in terms of two factors [1,4]. First, inclusion of impermeable crystallites decreases the amount of amorphous material through which the permeant can diffuse. Second, impermeable crystallites increase the tortuosity of the transport path (geometric impedance). The former affects total solubility of the permeant (Fig. 7(c)), the latter affects the diffusion coefficient. In the present study, the reduction in permeability was caused primarily by a decrease in the diffusion coefficient (Fig. 7(b)). The solubility coefficient showed insignificant initial drop within 0–0.07 of volume fraction of crystallinity, and then remained constant in spite of increase of crystalline fraction. Thus, the specific solubility of oxygen in the amorphous phase must have increased with crystallinity.

It is interesting to note that oxygen permeability for cold-

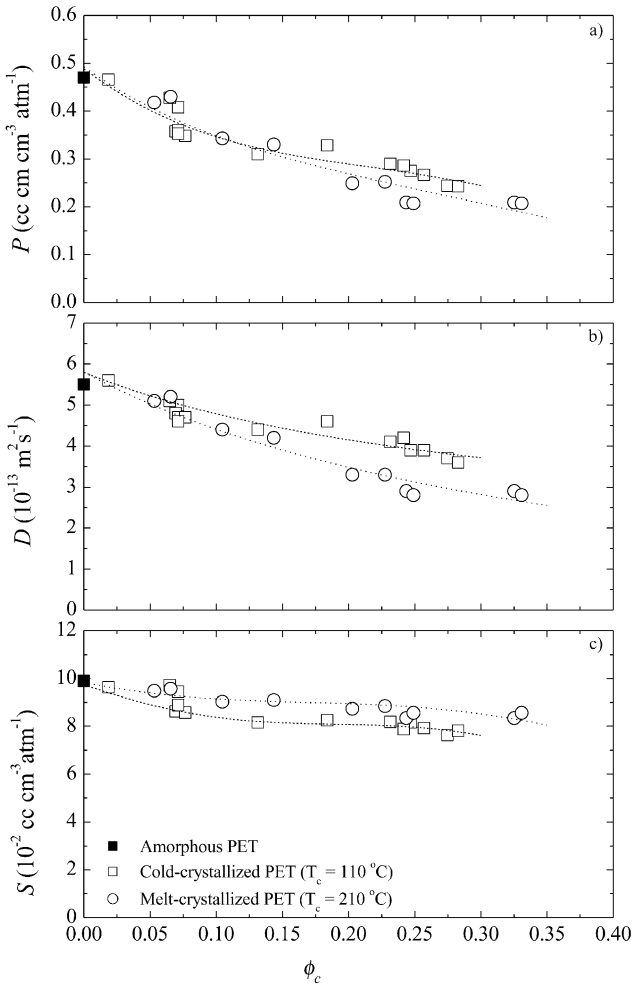

Fig. 7. Effect of volume fraction of crystallinity on oxygen permeability (a), diffusivity (b) and solubility (c) for cold-crystallized at 110 °C and melt-crystallized at 210 °C PET.

and melt-crystallized PET with the same crystallinity was very similar. However, the diffusion coefficient for melt-crystallized PET was slightly lower, while solubility was slightly higher than those for cold-crystallized PET.

3.3. Oxygen solubility of rigid amorphous phase

The apparent increase in oxygen solubility of the amorphous phase with crystallinity for both melt- and cold-crystallized PET can be understood: if to assume that MAF and RAF are characterized by different solubility coefficients, S_{MAF}, and S_{RAF}, respectively. Then, the overall solubility of the amorphous phase in semicrystalline PET can be naturally expressed as follows:

$$S = \phi_{MAF} S_{MAF} + \phi_{RAF} S_{RAF} \tag{4}$$

The oxygen solubility of MAF, S_{MAF}, was estimated from the measurements of oxygen permeation in the pure amorphous PET at 25 °C, $S_{am} = S_{MAF} = 0.095 \pm 0.002$ cc(STP) cm^{-3} atm^{-1}. Practically, the same solubility in the pure amorphous PET at 25 °C, $S_{am} = 0.098 \pm$

0.002 cc(STP) cm^{-3} atm^{-1} was also reported elsewhere [29]. Thus, if the overall solubility, S, for given volume fraction of crystallinity is known as well as the corresponding volume fractions of MAF and RAF, the solubility of RAF can also be calculated. Fig. 8 shows the plot of experimentally measured quantity $S - \phi_{MAF}S_{MAF}$ versus volume fraction of RAF, ϕ_{RAF} for melt-crystallized at 210 °C and cold-crystallized at 110 °C PET. Both experimentally measured dependencies were essentially linear. So, from the corresponding slopes of these linear dependencies, the solubility coefficients of RAF for melt- and cold-crystallized PET were estimated accordingly. The solubility coefficient of RAF in melt-crystallized at 210 °C PET was found to be 0.203 ± 0.014 cc(STP) cm^{-3} atm^{-1}. The solubility coefficient of RAF in cold-crystallized at 110 °C PET was found to be 0.119 ± 0.004 cc(STP) cm^{-3} atm^{-1}. This result shows that the solubility coefficient of RAF is larger than the solubility coefficient of MAF. Moreover, the solubility coefficient of RAF in melt-crystallized at 210 °C PET was found to be significantly larger than that in cold-crystallized at 110 °C PET. The last fact can explain why the overall solubility measured in melt-crystallized PET containing the same crystalline fraction was even slightly larger than that in cold-crystallized PET despite significantly smaller amount of RAF developed upon crystallization in the melt state.

Similarly, we estimated the solubility of RAF for PET isothermally cold-crystallized at 140 °C, 0.130 ± 0.006 cc(STP) cm^{-3} atm^{-1}, and cold-crystallized at 160 °C, 0.145 ± 0.007 cc(STP) cm^{-3} atm^{-1}. Therefore, oxygen solubility of RAF progressively increased with the increase of crystallization temperature.

3.4. Oxygen solubility and specific volume of the amorphous phase

It is well known that the thermal expansion coefficient α undergoes a jump $\Delta\alpha$ upon cooling below the glass transition temperature T_g (Fig. 9). Hence, the specific volume for the glassy state, v_g is larger than that for the supercooled liquid, v_l, at the same temperature T by an excess-hole free volume v_f

$$v_f = v_g - v_l = \Delta\alpha(T_g - T) \quad (5)$$

where $\Delta\alpha = \alpha_l - \alpha_g$ is the difference between thermal expansion coefficients of the equilibrium polymer melt and glass. The excess-hole free volume is usually ascribed to the packing defects frozen in the structure of polymer due to inhibiting the segmental mobility below T_g. The packing defects can be imagined as molecular size cavities where sorption of the gas molecules is considerably facilitated. This concept underlines the dual sorption model that distinguishes permeant molecules adsorbed in the cavities or 'holes', and those dissolved in the polymer matrix [1,2,19]. For oxygen in PET, it was shown that the contribution of the dissolution mechanism is small, and that the permeation molecules are mainly sorbed in holes [2]. In this case, sorption is the process of filling the holes, and the solubility coefficient should be proportional to the amount of excess-hole free volume, $S \sim v_f$. Assuming that the equilibrium polymer melt expansion is the unique feature of the polymer, v_l must be constant at given temperature T and the solubility coefficient in the glassy state has to be directly proportional to the specific volume of the glass $S \sim v_g$. The linear relationship between specific volume of the glassy amorphous polymer, v_g, and oxygen solubility, S, was demonstrated at 25 °C for PET and PET related copolymers by Polyakova et al. [29]. The slope of this linear correlation was found to be $\beta = 3.6$ cc(STP) g cm^{-6} atm^{-1}. When this dependence, $S(v_g)$, was extrapolated to $S = 0$, it gave the minimum of specific volume of amorphous polymer with no excess-hole free volume $v_{g,min} = v_l(25\,°C) = 0.722$ cm^3 g^{-1}. It was important to verify that this value indeed corresponded to the specific volume of supercooled down to RT equilibrium polymer melt.

PET is a semicrystalline polymer, which crystallizes and

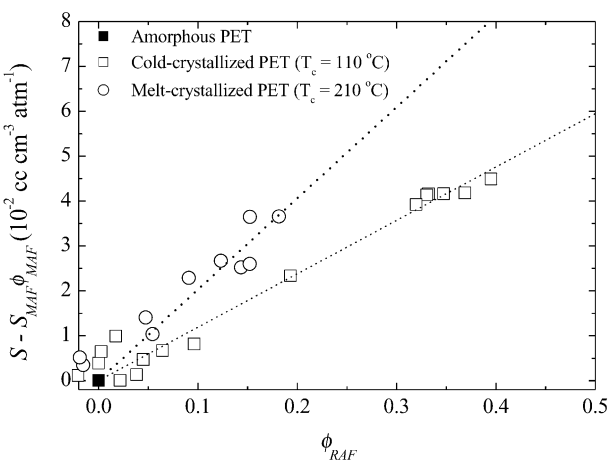

Fig. 8. Quantity $S - \phi_{MAF}S_{MAF}$ versus volume fraction of RAF, ϕ_{RAF}, for melt-crystallized at 210 °C and cold-crystallized at 110 °C PET.

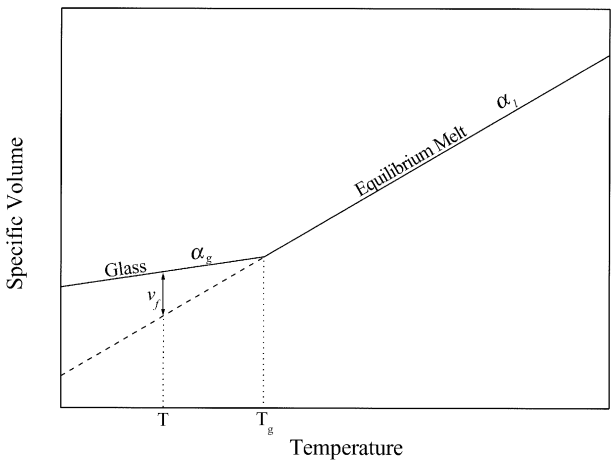

Fig. 9. Representation of the specific volume–temperature relationship for an amorphous polymer.

recrystallizes upon heating in a broad range of temperatures above the glass transition. These processes are associated with very significant change in the specific volume. Therefore, an accurate assessment of the equilibrium melt thermoexpansion, $v_l(T)$, for PET becomes virtually impossible in the range of temperatures above the glass transition temperature up to melting. Above the melting temperature, melt thermal expansion could be measured accurately but only within a relatively narrow temperature interval. The melting temperature of PET is relatively high and thermal degradation occurs soon after the melting leading to an additional increase of the specific volume associated with the formation of gaseous products of degradation reactions. Fig. 10 (filled symbols) shows the $v(T)$ diagram obtained at atmospheric pressure for highly crystalline PET (specific volume at ambient conditions 0.7194 $cm^3\ g^{-1}$). We used the data available in the monograph published by Zoller and Walsh, which is one of the most reliable sources of the PVT information for polymers [30]. As it can be clearly seen from the figure, the melt thermoexpansion process of PET alone can only be considered within a very narrow temperature interval, 270–320 °C, where $v(T)$ exhibits a constant slope about $5 \times 10^{-4}\ cm^3\ g^{-1}\ K^{-1}$. In the range 100–270 °C, the temperature dependence of a specific volume exhibit a very complex behavior associated with a number of concurrent processes such as thermal expansion of the amorphous and crystalline phases, and crystallization/recrystallization and melting of the crystalline phase. The range of temperatures above 320 °C is not reliable to measure the thermoexpansion of PET melt as well because the upswing of $v(T)$ is evidently associated with an onset of polymer degradation. The narrow temperature interval, where the melt thermal expansion of PET, $v_l(T)$, is only well defined, makes an extrapolation of the melt thermal expansion down to RT to be a subject of the great uncertainty in order to define the specific volume of supercooled polymer melt at RT, v_l (25 °C). However, in their monograph, Zoller and Walsh also reported the $v(T)$ diagram at atmospheric pressure for poly(ethylene isophthalate) (PEI), the terephthalate isomer of PET. PEI and PET exhibit the same molecular weight and chemical composition of the monomer unit. The only difference is that in more flexible PEI, the phenyl ring is attached to the polymer chain backbone in *meta*-position, while in more rigid PET the phenyl ring is attached in *ortho*-position. PEI, in comparison with PET does not crystallize. So, unperturbed by crystallinity, the melt thermoexpansion behavior of this chemically very similar to PET polymer is available within a very broad range of temperatures above the glass transition temperature. The $v(T)$ diagram for PEI is also shown in Fig. 10 (open symbols). The $v(T)$ diagrams for PET and PEI overlap very well above the melting temperature of PET. Naturally, we assumed that these diagrams would overlap below the melting temperature of PET if thermal expansion of pure amorphous PET was possible to measure within this temperature interval, except

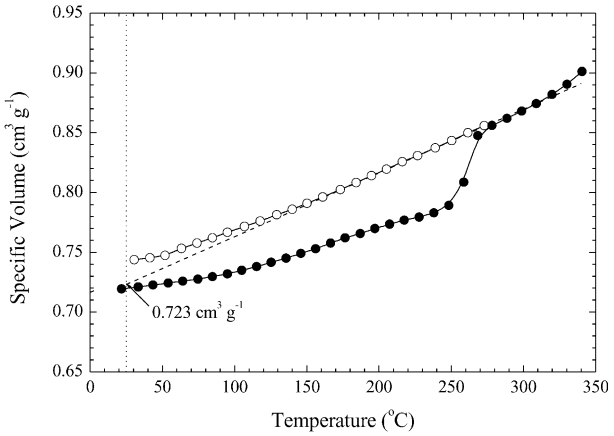

Fig. 10. Specific volume versus temperature for semicrystalline PET (filled symbols) and amorphous PEI (opened symbols). The data are taken from the monograph published by Zoller and Walsh [29].

may be the temperature interval close to T_g. At lower temperatures close to T_g, the difference in the chain rigidity of PET and PEI can start playing an important role eventually leading to vitrification of more rigid PET at higher temperatures. Thus, to extrapolate the melt thermoexpansion of PET down to RT we used the combined $v(T)$ data for PET and PEI in the temperature range 150–320 °C. In this broad range of temperatures, the melt thermoexpansion of this combined $v(T)$ diagram exhibits a very constant slope. It is interesting to note that below 150 °C, the slope $v(T)$ shows some decrease indicating an onset of the deviation from an equilibrium behavior. The slope obtained in the range 150–320 °C thus defines the thermal expansivity of the true equilibrium PET/PEI melt, $\alpha_l = (5.27 \pm 0.04) \times 10^{-4}\ cm^3\ g^{-1}\ K^{-1}$. It is interesting that Van Krevelen reported for PET significantly larger melt thermal expansivity $6.0/7.4 \times 10^{-4}\ cm^3\ g^{-1}\ K^{-1}$ [31]. However, it is not clear in this monograph how the melt thermal expansivity was experimentally determined. Von Hellwege et al. [32] reported for amorphous PET the melt thermoexpansivity $4.5 \times 10^{-4}\ cm^3\ g^{-1}\ K^{-1}$ measured by mercury dilatometer. This value of melt thermal expansivity in turn is slightly smaller than that we claim in this work. However, Von Hellwege et al. [32] measured α_l for amorphous PET in very narrow range of temperatures (80–100 °C), slightly above T_g but below the cold-crystallization range. This certainly can explain why the reported in their work melt thermal expansivity for PET was found to be smaller than what we consider for PET in this work. Getting back to the value of α_l for PET reported by Van Krevelen, it seems interesting to note that Van Krevelen also reported, in addition to PET, the melt thermal expansivity for a number of other PET related copolymers such as poly(decamethylene terephthalate), PEI, poly[ethylene(2.6-naphthalate)], poly[ethylene(2.7-naphthalate)]. For all these polymers, the melt thermal expansivity is surprisingly similar, $4.9–5.3 \times 10^{-4}\ cm^3\ g^{-1}\ K^{-1}$, except for PET. It seems

Table 1
The effect of the crystallization temperature on solubility and specific volume of RAF

	Crystallization temperature (°C)	S_{RAF} (cc(STP) cm^{-3} atm^{-1})	Measured specific volume (cm^3 g^{-1})	Predicted specific volume (cm^3 g^{-1})
Cold-crystallized PET	110	0.119 ± 0.004	0.756 ± 0.001	0.754
	140	0.130 ± 0.006	0.759 ± 0.003	0.761
	160	0.145 ± 0.007	0.763 ± 0.003	0.766
Melt-crystallized PET	210	0.203 ± 0.014	0.779 ± 0.004	0.781

reasonable to admit that α_l for PET has to fall in this range of thermal expansivities as well.

After the melt thermoexpansion for PET was established within a broad range of temperatures, an accurate extrapolation of the equilibrium melt thermoexpansion down to 25 °C became possible (dotted line in Fig. 10). From this extrapolation, we determined the value of specific volume for supercooled down to 25 °C equilibrium melt $v_l(25\,°C) = 0.723$ cm^3 g^{-1}. This value was found to be in excellent agreement with the minimum of specific volume for amorphous PET or PET related copolymers at 25 °C with no excess-hole free volume $v_{g,min} = v_l(25\,°C) = 0.722$ cm^3 g^{-1} obtained by Polyakova et al. [29] using oxygen solubility data. Therefore, the empirical universal relationship obtained by Polyakova et al. was verified and used in this work to calculate the specific volume of the rigid amorphous phase, v_{RAF}, from the oxygen solubility calculated for RAF

$$v = v_l(25\,°C) + S/\beta \quad (6)$$

where $v_l(25\,°C) = 0.723$ cm^3 g^{-1}, $\beta =$ cc(STP) g cm^{-6} atm^1, S is oxygen solubility expressed in cc(STP) cm^3 atm^1.

It is interesting to hypothesize here why oxygen solubility for PET and the large group of PET related copolymers obeyed so well the linear relationship expressed by Eq. (6). In part, this universal relationship could be explained assuming that all PET related copolymers obtained by replacing the terephthalic group exhibited very similar dependence of the specific volume versus temperature in the melt state, as it seems to be the case for PET and PEI. Then, this universal melt thermal expansion should lead automatically to the universal for these PET related copolymers value of the amorphous specific volume with no excess-hole free volume at 25 °C, v_l (25 °C). The question, however, remains why the coefficient β in Eq. (6) is also a sort of universal constant for the various PET-based copolymers.

3.5. Specific volume of rigid amorphous fraction

Table 1 shows oxygen solubilities and calculated using Eq. (6) specific volumes of RAF for melt-crystallized at 210 °C and cold-crystallized at 110, 140, 160 °C PET. As expected, specific volume of RAF increased with an increase of crystallization temperature. For comparison, the specific volume of RAF for the melt-crystallized at 210 °C PET was by 4.0% larger than that for the completely amorphous PET containing only MAF. In turn, the specific volume corresponding to the pure MAF was only by 3.6% larger than the specific volume corresponding to the supercooled PET melt at 25 °C containing no excess-hole free volume. Therefore, an increase of the specific volume of RAF is significant.

Now, it became possible to check whether the hypothesis previously proposed by Schick et al. [17,18] suggesting that the crystallization temperature T_c corresponded to the vitrification temperature for RAF, was right. Fig. 11 shows a procedure for prediction of specific volume of RAF at 25 °C using the combined dependence of specific volume versus temperature for PET/PEI melt. The points on this melt thermoexpansion diagram were fixed at the crystallization temperatures 110, 140, 160 and 210 °C. Then, with a constant slope corresponding to the thermoexpansion coefficient of PET in the glassy state, α_g, the extrapolation was made down to the RT 25 °C. We found the predicted specific volumes of RAF (Table 1) and the specific volumes of RAF, which was determined using the oxygen solubility data to be the same within the experimental accuracy for $\alpha_g = 2.2 \times 10^{-4}$ cm^3 g^{-1} K^{-1}. This value of α_g is within the reported range of glass thermal expansion coefficient for PET $1.8–2.4 \times 10^{-4}$ cm^3 K^{-1} g^{-1} [31–33].

This result confirmed that upon crystallization from either melt or glassy state, the constrained between the crystalline lamellas amorphous PET chains indeed become

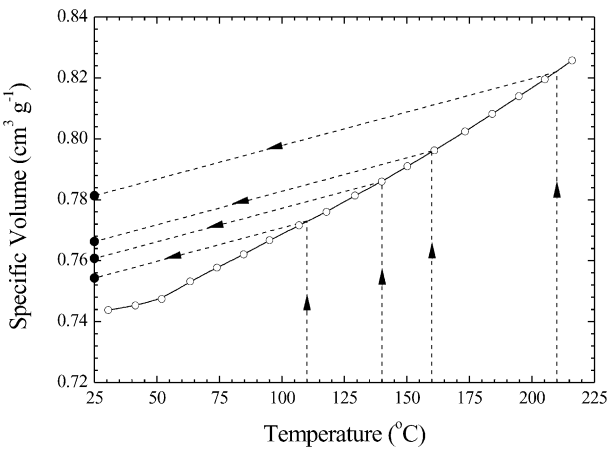

Fig. 11. Procedure for calculating specific volume of RAF at 25 °C for PET melt- and cold-crystallized at various temperatures.

vitrified at the crystallization temperature. Therefore, the rigid amorphous fraction even below the crystallization temperature preserves a memory about the melt state, which is uniquely defined by the crystallization temperature. It is not exactly clear what is the mechanism responsible for the constrained between crystalline lamellas amorphous chains to become vitrified despite the high temperature of the melt. Considering an analogy with a polymer network, where T_g is increased due to inhibiting of segmental mobility as compared with an uncrosslinked polymer, we can hypothesize that segmental mobility of chains constrained between narrow-spaced crystalline lamellas could also become severely hindered to the extent that the RAF vitrifies despite high temperature.

It was interesting to check in the end whether the overall density of semicrystalline PET can be predicted from the phase model consisting of the crystalline, mobile and rigid amorphous fractions. Fig. 12 shows the calculated overall density versus experimentally measured density for PET melt crystallized at 210 °C and cold-crystallized at 110 °C. For comparison, the density was calculated using two-phase model (open symbols) and three-phase model (filled symbols). In the two-phase model, we assumed that no rigid amorphous fraction is present, and the densities of crystalline and amorphous phases are constant, 1.515 and 1.335 g cm^{-3}, respectively. In the three-phase model, we assumed that the amorphous phase consists of the MAF with a constant density 1.335 g cm^{-3} and the RAF, for which the density was calculated using the oxygen solubility data, $\rho_{RAF} = 1.323$ g cm^{-3} ($T_c = 110$ °C), $\rho_{RAF} = 1.284$ g cm^{-3} ($T_c = 210$ °C). The density for 100% crystalline phase in the three-phase model was assumed 1.515 g cm^{-3}. As in the case of heat capacity jump, ΔC_p, at T_g the deviation from the two-phase model is clearly observed for melt- and cold-crystallized PET starting at about 10% volume fraction of crystallinity ($\rho = 1.350$ g cm^{-3}). This is presumably associated with the formation of less dense RAF. This deviation levels off at about 20% volume fraction of crystallinity ($\rho = 1.365$ g cm^{-3}) in agreement with saturation of the amount of the RAF with crystallinity (Fig. 5(b)). The densities predicted from the three-phase model showed a good agreement with the experimentally measured densities in contrast with the prediction of the two-phase model.

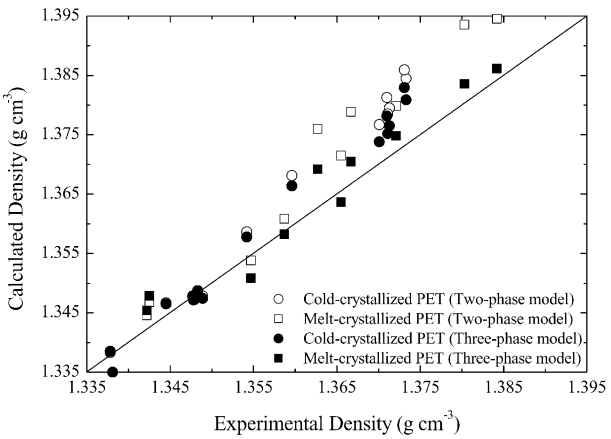

Fig. 12. Calculated from two-phase model (opened symbols) and three-phase model (filled symbols) overall density versus experimentally measured density for cold-crystallized at 110 °C and melt-crystallized at 210 °C PET.

4. Conclusions

It was shown that gas solubility measurements could be employed as an effective tool to probe the packing of polymer chains in the glassy, amorphous phase. Vitrification of amorphous polymer is associated with the formation of excess-hole free volume, packing defects effectively frozen in the structure of polymer due to drastic restriction of the macromolecular segmental mobility. These defects (molecular size holes) act as the adsorption sites where gas sorption is considerably stronger than in the dense polymer matrix containing no excess-hole free volume. If the relationship between gas solubility and excess-hole free volume is known as well as the specific volume of dense polymer matrix containing no excess-hole free volume, the specific volume of glassy, amorphous polymer can be accurately determined from gas solubility measurements.

Explanation of unexpectedly high oxygen solubility observed in semicrystalline PET was attributed to the formation of RAF, which in comparison with mobile or regular amorphous fraction is constrained between crystalline lamellas and vitrifies at higher than T_g temperature. This results in extra excess-hole free volume developed by the RAF upon cooling and subsequently larger oxygen solubility of this amorphous fraction.

Measurements of crystallinity and jump in the heat capacity at T_g were used to determine the amount of mobile and rigid amorphous fractions in semicrystalline PET. Overall oxygen solubility was considered to consist of two independent contributions, the solubility of MAF and the solubility of RAF. The oxygen solubility of the RAF was determined and the specific volume of this amorphous fraction was calculated at RT. The oxygen solubility and the specific volume of RAF showed a direct correlation with the crystallization temperature. Whether PET was cold-crystallized or melt-crystallized had no effect on oxygen solubility or specific volume of the RAF.

A model, which assumed that vitrification of the RAF in semicrystalline PET occurs at crystallization temperature was considered. The model made it possible to make a prediction of the specific volume of the RAF. The predicted values of the specific volume for PET crystallized at various temperatures and the specific volume data obtained using oxygen solubility measurements showed an excellent agreement. This result confirmed that vitrification of the RAF in semicrystalline PET occurs at crystallization temperature.

Acknowledgments

The authors thank Prof. A. Hiltner for many stimulating discussions. The research was generously supported by the KOSA Corp. and National Science Foundation through Grant DMR-9986467 and Grant DMR-9975774 (Polymer Program, Division of Material Research). Support from Modern Controls, Inc. for development of a facility for gas-transport studies at Case Western Reserve University is gratefully acknowledged.

References

[1] Vieth WR. Diffusion in and through polymers. Munich: Hanser; 1991.
[2] Michaels AS, Vieth WR, Barrie J. J Appl Phys 1963;34:1.
[3] Sekelik DJ, Stepanov EV, Nazarenko S, Schiraldi D, Hiltner A, Baer E. J Polym Sci, Part B: Polym Phys 1999;37:847.
[4] Hedenquist M, Gedde UW. Prog Polym Sci 1996;21:299.
[5] Bornschleg E, Bonart R. Colloid Polym Sci 1980;258:319.
[6] Schlosser E, Schonhals A. Colloid Polym Sci 1989;267:963.
[7] Cheng SZD, Cao M-Y, Wundelich B. Macromolecules 1986;19:1868.
[8] Huo P, Cebe P. Macromolecules 1992;25:902.
[9] Cheng SZD, Wu Z, Wunderlich B. Macromolecules 1987;20:2802.
[10] Huo P, Cebe P. J Polym Sci Polym, Phys Ed 1992;30:239.
[11] Abis L, Merlo E, Po R. J Polym Sci, Part B: Polym Phys 1995;33:691.
[12] Cheng SZD, Wundelich B. Macromolecules 1988;21:789.
[13] Lovinger AJ, Hudson SD, Davis DD. Macromolecules 1992;25:1992.
[14] Santa Cruz C, Stribeck N, Zachmann HG, Balta Calleja FJ. 1991; 24:5980.
[15] Sauer BB, Hsiao BS. Polymer 1995;36:2553.
[16] Seyler RJ. J Therm Anal 1997;49:491.
[17] Schick C, Dobbertin J, Potter M, Dehne H, Hensel A, Wurm A, Ghoneim AM, Weyer S. J Therm Anal 1997;49:499.
[18] Schick C, Wurm A, Mohamed A. Colloid Polym Sci 2001;279:800.
[19] Petropoulos JH. In: Paul DR, Yampol'skii YP, editors. Polymer gas separation membranes. Ann Arbor: CRC Press; 1994. p. 17.
[20] Rehage G, Borchard W. In: Haward RN, editor. The physics of glassy polymers. New York: Halsted Press; 1973. p. 54.
[21] Richardson MJ. In: Mathot VBF, editor. Calorimetry and thermal analysis of polymers. Munich: Hanser; 1993. p. 170.
[22] Wunderlich B, Macromolecular physics, vol. 1. New York: Academic Press; 1973. p. 389.
[23] Grebowicz J, Lau SF, Wunderlich BJ. J Polym Sci, Polym Symp 1984;71:19.
[24] Suzuki H, Grebowicz J, Wunderlich BJ. Macromol Chem 1985;186: 1109.
[25] Brandrup J, Immergut EH. Polymer handbook, 3rd ed. New York: Wiley-Interscience; 1989.
[26] de P. Daubeny R, Bunn CW, Brown CJ. Proc R Soc Lond Ser A 1954; 226:531.
[27] Kilian HG, Halboth H, Jenckel E. Kolloid Z 1960;172:166.
[28] Fakirov S, Fischer EV, Schmidt GF. Macromol Chem 1975;176:2459.
[29] Polyakova A, Liu RY, Schiraldi DA, Hiltner A, Baer E. J Polym Sci, Part B: Polym Phys 2001;39:1889.
[30] Zoller P, Walsh DJ. Standard pressure–volume–temperature data for polymers. Basel: Technomic; 1995.
[31] Van Krevelen DW, 3rd ed. Properties of polymers, vol. 1. Amsterdam: Elsevier; 1997. p. 71.
[32] Von Hellwege K-H, Hennig J, Knappe W. Kolloid Z 1962;186:29.
[33] Sharma SC, Mandelkern L, Stehling FC. Polym Lett 1972;10:345.